Journal of
Applied Crystallography

ISSN 0021-8898

Received 25 February 2005
Accepted 8 October 2005

The spatial structure of dendritic macromolecules

A. N. Ozerin,[a]* D. I. Svergun,[b] V. V. Volkov,[c] A. I. Kuklin,[d] V. I. Gordelyi,[d] A. Kh. Islamov,[d] L. A. Ozerina[a] and D. S. Zavorotnyuk[a]

[a]Institute of Synthetic Polymer Materials, Moscow, Russia, [b]European Molecular Biology Laboratory, c/o DESY, Hamburg, Germany, [c]Institute of Crystallography, Moscow, Russia, and [d]Joint Institute for Nuclear Research, Dubna, Russia. Correspondence e-mail: ozerin@ispm.ru

A low-resolution *ab initio* shape determination was performed from small-angle neutron and X-ray scattering (SANS and SAXS) curves from solutions of polycarbosilane dendrimers with the three-functional and the four-functional branching centre of the fourth, fifth, sixth, seventh and eighth generations. In all cases, anisometric dendrimer shapes were obtained. The overall shapes of the dendrimers with the three- and four-functional branching centres were oblate ellipsoids of revolution and triaxial ellipsoids, respectively. The restored bead models revealed a pronounced heterogeneity within the dendrimer structure. The density deficit was observed in the central part and close to the periphery of the dendrimers. The fraction of the overall volume of the dendrimers available for solvent penetration was about 0.2–0.3. These results may help in the design of new practical applications of dendrimer macromolecules.

1. Introduction

Detailed knowledge of the spatial structure of dendritic (tree-like, highly branched) macromolecules is important in order to design challenging new practical applications (Fréchet & Tomalia, 2001) based on the principles of host–guest and supramolecular chemistry. At present, no consensus model of dendritic structure formation is available (Ozerin *et al.*, 2003). There are many unresolved problems in the structure determination of such nano-sized objects, even for the case of dendritic macromolecules of the regular chemical structure (dendrimers). The main reason is that the interpretation of the experimental results is highly dependent on the *a priori* model selected to represent the spatial structure. This is why, for example, the density distribution within the dendrimers of different generations and in particular of the dendrimer interactions in solution remain the subject of intensive investigations (Topp *et al.*, 1999; Likos *et al.*, 2001; Prosa *et al.*, 2001; Ramzi *et al.*, 2002; Mallamace *et al.*, 2002). It is thus important to use approaches working with the experimental information *ab initio* (Ozerin *et al.*, 2004) to build a model-independent picture of the internal dendrimer structure.

The present paper presents the results of the restoration of the low-resolution shape and internal structure of polycarbosilane dendrimers in solution from small-angle neutron scattering (SANS) and small-angle X-ray scattering (SAXS) data, made without *a priori* information on the dendrimer's structure (*ab initio*). A new model of the dendrimer spatial structure is proposed, taking into account the possibility of solvent-molecule penetration inside the dendrimer macromolecules.

2. Experimental

The synthesis and characterization of the polycarbosilane dendrimers has been described elsewhere (Ponomarenko *et al.*, 1998; Tatarinova *et al.*, 2004). The fourth, fifth, sixth, seventh and eighth generations (G4–G8) were investigated for the two types of dendrimers: (i) with the three-functional phenyl-substituted silicone core [$G^{(3)}5$–$G^{(3)}7$] and (ii) with the four-functional silicone core [$G^{(4)}4$–$G^{(4)}8$]. All of the above dendrimers were purified by a preparative SEC (size exclusion chromatography) device consisting of a isocratic high-pressure pump 'Stayer' (Acvilon), Phenogel 10 μm preparative columns, 300 × 21.2 mm, of 10 × 3 Å or 10 × 5 Å pore size (Phenomenex Ltd), and a RIDK-102 refractometer detector (Ecom). Tetrahydrofuran was used as eluent. Thus the chromatographic purity of all the samples under investigation was provided. The structure of the dendrimers for the (smaller than investigated) generations $G^{(3)}3$ and $G^{(4)}3$ is shown schematically in Fig. 1 in a two-dimensional representation, to give more insight into the spatial arrangement of the higher generations G4–G8 (the latter would be more difficult to draw in two dimensions).

The chemical compositions of the dendrimers could be realised from the molecular formulae and the molecular mass values shown in Table 1.

The bulk density of the dendrimers, measured by a bottle method, ranged from 0.88 g cm^{-3} to 0.91 g cm^{-3} (Kuklin *et al.*, 2003).

The SANS experiments for the $G^{(3)}5$–$G^{(3)}7$ and $G^{(4)}5$–$G^{(4)}7$ dendrimers were performed at the YuMO instrument, equipped with a two-detector system (Kuklin *et al.*, 2002), at the IBR-2 reactor of FLNPh JINR (Dubna). The time-of-flight

Table 1
Characteristics of the dendrimers.

M = calculated molecular mass; R_g = radius of gyration (nm) calculated with the program *GNOM* from SANS and SAXS; *a*:*b*:*c* = semi-axes of the equivalent ellipsoid restored with the program *SASHA*; V_{env} = volume of the equivalent ellipsoid (nm^3) restored with the program *SASHA*; V_{DAM} volume of the bead model body (nm^3) restored with the program *DAMMIN*.

Sample	Molecular formula	M	R_g	*a*:*b*:*c*	V_{env}	V_{DAM}
$G^{(3)}5$	$Si_{94}C_{666}H_{1322}$	11971	1.9	1.7:1.7:1	52	40
$G^{(3)}6$	$Si_{190}C_{1338}H_{2666}$	24093	2.0	2.2:1.8:1	54	45
$G^{(3)}7$	$Si_{382}C_{2682}H_{5354}$	48337	2.2	1.8:1.8:1	95	76
$G^{(4)}4$	$Si_{61}C_{496}H_{1116}$	8796	1.7	2.4:1:1	16	13
$G^{(4)}5$	$Si_{125}C_{1008}H_{2270}$	17904	2.1	2.4:1:1	45	34
$G^{(4)}6$	$Si_{253}C_{2032}H_{4572}$	36120	2.4	2.3:1:1	92	54
$G^{(4)}7$	$Si_{509}C_{4080}H_{9180}$	72554	2.9	2.4:1.6:1	160	100
$G^{(4)}8$	$Si_{1021}C_{8176}H_{18396}$	145421	3.1	2.3:1.6:1	207	160

counting method was used, with the first detector placed at a sample–detector distance of 5.28 m and the second one at 13.04 m to give the overall range of momentum transfer of $0.08 < s = 4\pi\lambda^{-1}\sin\theta < 4\ \mathrm{nm}^{-1}$, where 2θ is the scattering angle and λ is the wavelength. The averaged scattering patterns were corrected with respect to detector response, absorption, solvent scattering and instrumental background, and converted into the elastic scattering cross section on the absolute intensity scale $I(s)$ using vanadium as a standard.

The SANS measurements were performed with diluted solutions (1–2 wt%) of the dendrimers in benzene-d_6, at 298 K.

The neutron scattering length density ρ_{sol} of the solvent was $5.44 \times 10^{10}\ \mathrm{cm}^{-2}$ (benzene-d_6). The neutron scattering length densities ρ_d of the dendrimers calculated from their chemical structure and the bulk density values amounted to $-0.06 \times 10^{10}\ \mathrm{cm}^{-2}$ [$G^{(3)}5$–$G^{(3)}7$] and $-0.37 \times 10^{10}\ \mathrm{cm}^{-2}$ [$G^{(4)}4$–$G^{(4)}8$]. The solutions were placed into standard cuvettes (Hellma) with a thickness of 1 mm in the direction of the neutron beam.

In addition to the SANS measurements, SAXS measurements for the $G^{(4)}4$ and $G^{(4)}8$ dendrimers were made using a KRM-1 camera (Bourevestnik Inc.) with a slit collimation system (Cu $K\alpha$ radiation, Ni filter, scintillation counter), giving an overall range of momentum transfer of $0.07 < s = 4\pi\lambda^{-1}\sin\theta < 4.26\ \mathrm{nm}^{-1}$. The SAXS measurements were performed with diluted solutions (2 wt%) of the dendrimers in hexane at 298 K. The dilute solutions of the dendrimers in hexane were placed in glass capillaries (Hilgenberg GmbH) for SAXS measurements.

Prior to the analysis, the data were smoothed, corrected for absorption, solvent scattering, instrumental background and slit-length smearing, utilizing the program packages *SYRENA* and *GNOM* (Feigin & Svergun, 1987; Svergun, 1991, 1992). SANS and SAXS measurements are complementary to each other for the studied dendrimers, as was shown previously (Kuklin *et al.*, 2003).

The influence of the interparticle interference was found to be negligible for the diluted (1–2 wt%) solutions of the studied dendrimers (Kuklin *et al.*, 2002, 2003; Ozerin *et al.*, 2004) and the coherent scattering intensity $I(s)$ was defined in this case mainly by the rotationally averaged scattering intensity from a single particle (Feigin & Svergun, 1987). The radius of gyration values, R_g, calculated with the program *GNOM* (Svergun, 1992) from the small-angle scattering (SAXS) data, are indicated in Table 1.

The programs *PRIMUS* (Konarev *et al.*, 2003), *GNOM* (Svergun, 1991, 1992), *MASHA* (Konarev *et al.*, 2001), *SASHA* (Svergun *et al.*, 1996) and *DAMMIN* (Svergun, 1999) of the *ATSAS2.0* program package (available from www.embl-hamburg.de/ExternalInfo/Research/Sax) were used for the data treatment and structure evaluation.

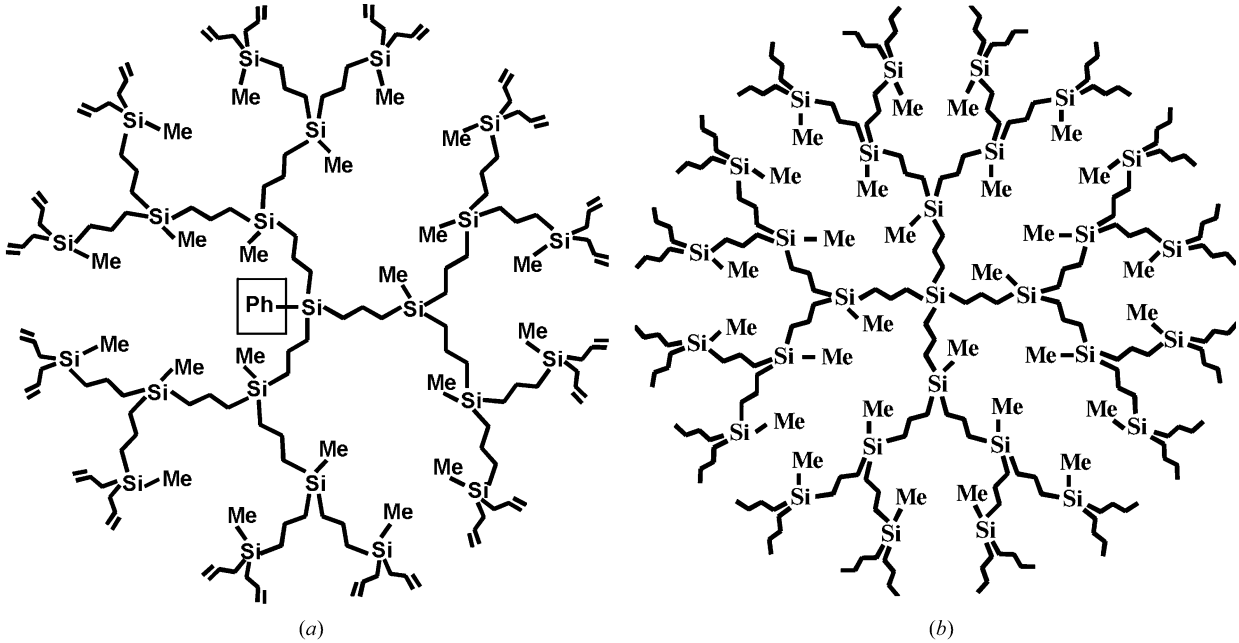

Figure 1
Schematic structure of $G^{(3)}3$ (*a*) and $G^{(4)}3$ (*b*) dendrimers in a two-dimensional representation.

The program *PRIMUS* performs manipulations with experimental SAS data files (such as averaging, subtraction, merging, extrapolation to zero concentration and curve fitting) and evaluates the integral parameters from Guinier and Porod plots (such as radius of gyration, Porod's volume, zero intensity and molecular weight). The program *GNOM* is an indirect transform program for SAS data processing. The program *SASHA* implements an envelope determination technique. This program was run in a batch mode using the default parameters without symmetry restrictions (*P*1). For *SASHA*, the multipole resolution of $L = 3$ and $L = 4$ was used, where L is the maximum order of the spherical harmonics. The Monte Carlo type simulated-annealing program *DAMMIN* was used to reconstruct the shapes of the dendrimers. The program was run in a batch mode using the default parameters. The shapes were reconstructed without symmetry (*P*1) and also with different symmetry restrictions (point groups *P*2, *P*22, *P*23, *P*3, *P*32, *P*422, *P*432). The *DAMMIN* calculations were made in a 'fast' (fewer beads) as well as in a 'slow' (more beads) mode. For automated analysis of independent *DAMMIN* reconstructions, the program package *DAMAVER*, based on the program *SUPCOMB* (Kozin & Svergun, 2001), was used. For each model body, at least ten independent *DAMMIN* reconstructions were analysed by *DAMAVER*. The programs *MASSHA* and *RasMol* (v.2.7.1.1; http://www.bernstein-plus-sons.com/software/Rasmol_2.7.1.1) were used for three-dimensional rendering and manipulation of the low-resolution models, represented as smooth envelopes or ensembles of beads.

The χ^2 factor value was used to estimate goodness-of-fit of the experimental data against the scattering model intensity $I_{\rm cal}$ by calculating

$$\sum_{i=1}^{M}\left[\frac{I(s_i)-I_{\rm cal}(s_i)}{\Delta I(s_i)}\right]^2\frac{1}{M-M_{\rm par}}=\chi^2,$$

where M is the number of points at which the experimental intensities $I(s_i)$ were measured with error values $\Delta I(s_i)$, and $M_{\rm par}$ is the number of optimized parameters, including linear dimensions of the scattering particle, the coefficient for the background intensity subtraction and the adjustable scale factor.

3. Results and discussion

Fig. 2 represents the experimental SANS and SAXS curves for the dendrimers studied.

Only a few parameters of the scattering particle (radius of gyration, volume, maximum particle diameter) can be directly evaluated from the SANS and SAXS data. As a rule, further analysis by trial-and-error modelling requires *a priori* information and can by no means guarantee uniqueness. For example, the scattering curves from the model bodies in Fig. 2 [uniform ball and 'core–shell' model with the same value of $R_{\rm g}$ = 2.2 nm as for the $G^{(3)}7$ dendrimer] are different and reveal only the local approximation of the experimental SANS curve, while having the same χ^2 factor. In turn, the calculated scattering curves from the system of polydisperse particles with the well known form factors (sphere, ellipsoid, prism) never fitted the experimental scattering curves in the region of the form-factor maxima in Fig. 2, even for the best fits. Taking into account that the polydispersity in the molecular weight of the studied dendrimers was adequately eliminated during the sample preparation (Tatarinova *et al.*, 2004), further calculations and fits were made under the assumption of scattering from an ensemble of non-interacting (diluted) monodisperse particles. Recently, the modern *ab initio* shape determination methods in small-angle scattering were employed successfully in practice and checked on the uniqueness of shape determination (Volkov & Svergun, 2003). Starting with this approach, the method of angular envelope functions implemented in the computer program *SASHA* (Svergun *et al.*, 1996) and a bead modelling method implemented in the *ab initio* Monte Carlo type simulated-annealing program *DAMMIN* (Svergun, 1999; Volkov & Svergun, 2003) were used for the purpose of dendrimer shape determination in this work.

The results of the shape determination for the entire set of studied dendrimers, which are consistent with the preliminary results for the $G^{(3)}7$ and $G^{(4)}7$ dendrimers published recently (Ozerin *et al.*, 2004), are shown in Figs. 3 and 4.

All dendrimers were found to have essentially anisometric shapes by both *ab initio* programs, *SASHA* and *DAMMIN*

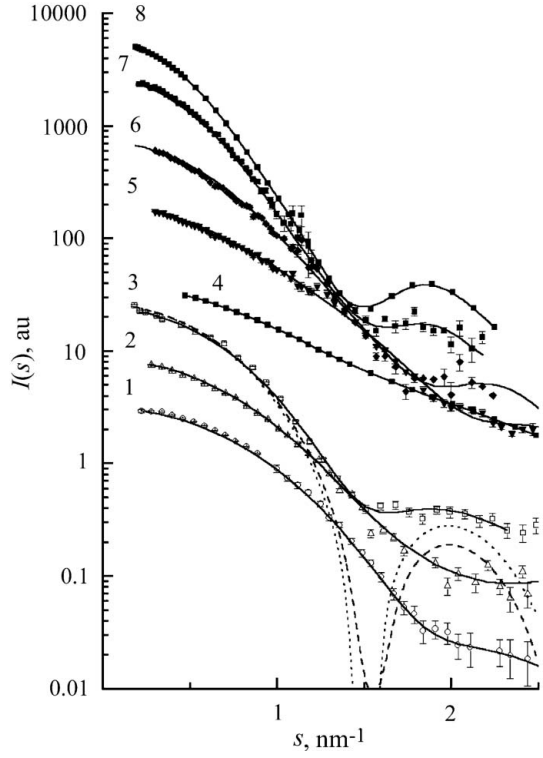

Figure 2
SAS curves for $G^{(3)}5$ (1), $G^{(3)}6$ (2), $G^{(3)}7$ (3), $G^{(4)}4$ (4), $G^{(4)}5$ (5), $G^{(4)}6$ (6), $G^{(4)}7$ (7) and $G^{(4)}8$ (8) dendrimers in diluted solutions. (1)–(3) and (5)–(7): SANS; (4) and (8): SAXS. Solid lines represent the fits of SAS data by the scattering of the model bodies restored by the programs *SASHA* and *DAMMIN*. Dashed and dotted lines correspond to the scattering from a uniform ball (R = 2.8 nm) and from a 'core–shell' model ($R1$ = 0.8, $R2$ = 2.8 nm), respectively.

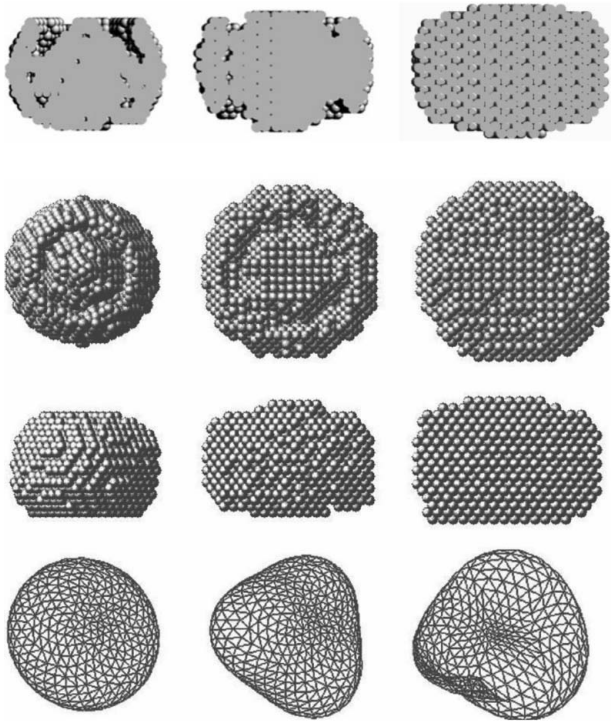

Figure 3
Shape determination for $G^{(3)}$ dendrimers. From left to right: $G^{(3)}5$, $G^{(3)}6$, $G^{(3)}7$. From top to bottom: equatorial cross section, front view, side view (*DAMMIN*); shape envelope (*SASHA*).

(except when running *DAMMIN* with symmetry *P*432; see below). This finding agrees with our earlier result (Kuklin *et al.*, 2003). The shape of an oblate ellipsoid of revolution was revealed for the $G^{(3)}$ type of dendrimers and that of a triaxial ellipsoid for the $G^{(4)}$ type of dendrimers (see Figs. 3 and 4, and Table 1 for details). The bead models of the dendrimers in Figs. 3 and 4 allow direct determination of their maximal (R_{max}) and minimal (R_{min}) linear dimensions and calculation of the appropriate moments of inertia (I_{max} and I_{min}). The calculated anisometric factors (R_{max}/R_{min}) and (I_{max}/I_{min}) are presented in Fig. 5.

The excluded particle volumes given by the program *DAMMIN* can be used for further validating the obtained models against the additional information. Fig. 6 displays the comparison of the restored excluded volume with the values calculated from the experimental bulk density and the molecular masses (Table 1) for the same dendrimers. As one can see from Fig. 6, the values provided by *DAMMIN* correlate well with the values predicted from the density measurements. This adds further credit to the models and numerical characteristics of the dendrimers reconstructed *ab initio*.

It is worth mentioning here that all the studied dendrimers never reached their upper limiting generation number. The excluded volume values for all the dendrimers were well below the limiting volume of a ball with the radius equal to the length of a fully straightened dendrimer's branch (see dotted line in Fig. 6).

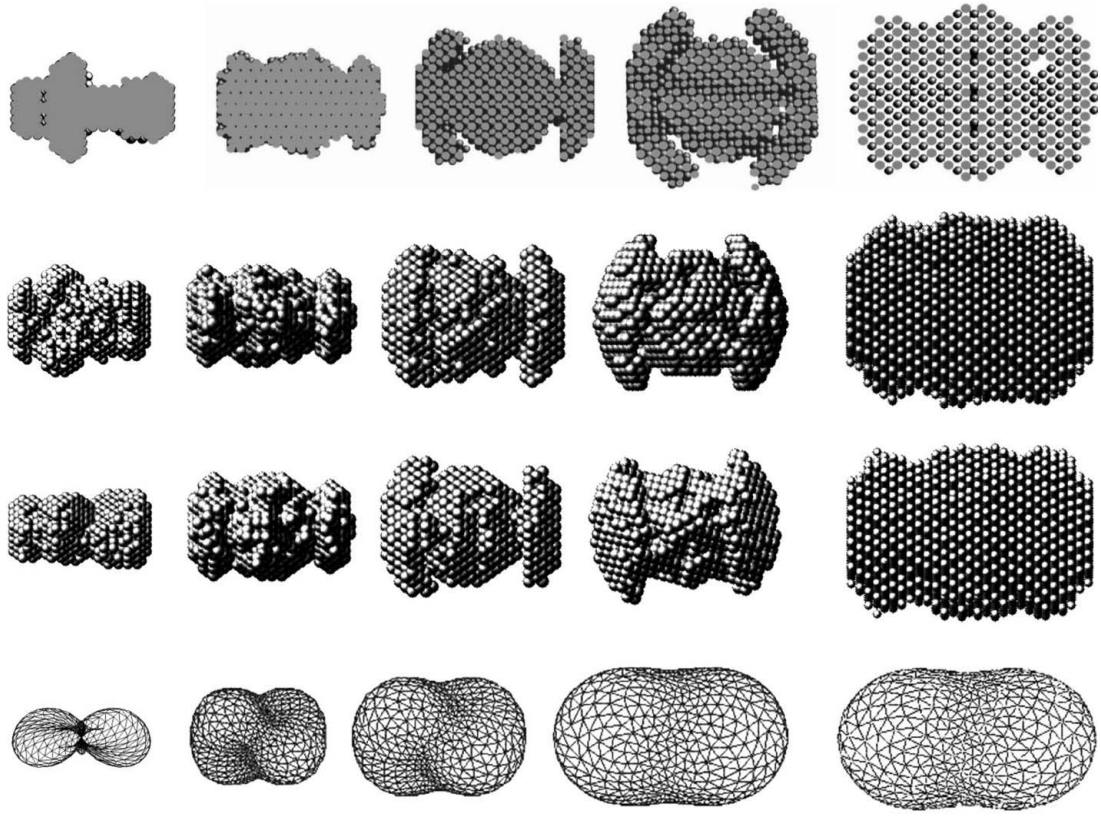

Figure 4
Shape determination for $G^{(4)}$ dendrimers. From left to right: $G^{(4)}4$, $G^{(4)}5$, $G^{(4)}6$, $G^{(4)}7$ and $G^{(4)}8$. From top to bottom: equatorial cross section, front view, side view (*DAMMIN*); shape envelope (*SASHA*).

In an attempt to verify the anisometric shapes of the dendrimers, their shape reconstruction was performed imposing different symmetry restrictions on the possible model. In all cases that included the lack of symmetry (group *P*1), the reconstructed shapes were similarly anisometric, the only exception being the cubic group with the symmetry *P*432 [see results in Fig. 7 for the $G^{(4)}7$ dendrimer as an example].

In this special case, the calculated SAS curves fitted the experimental curves with the same accuracy as for the anisometric shapes. However, the dendrimer shape restored under the assumption of the symmetry *P*432 appears to be rather artificial and could hardly be rationalized in terms of a dendrimer assembly. Moreover, it contradicts the hydrodynamic behaviour of the dendrimers in solution (Scherrenberg *et al.*, 1998; Sagidullin *et al.*, 2002), which is indicative of a compact (space-filling) structure and not of a loose permeable one. Given these data, the symmetric model in Fig. 7 can definitely be discarded. The possibility of building such a model compatible with the scattering data, is, however, an interesting example underlying the ambiguity of SAXS/SANS data interpretation and the necessity of accounting for additional information to reach unambiguous conclusions.

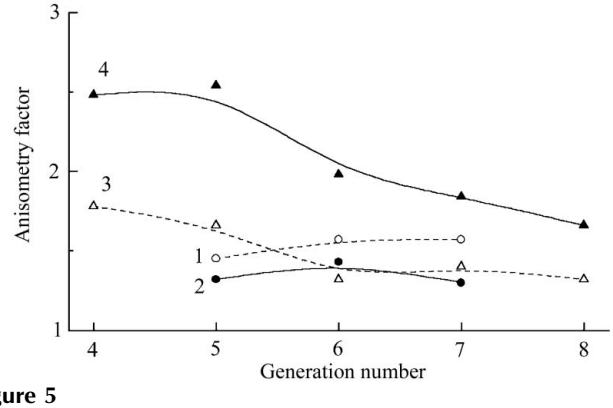

Figure 5
Anisometry factor for $G^{(3)}$ (1, 2) and $G^{(4)}$ (3, 4) dendrimers of different generations found from R_{max}/R_{min} (dashed lines) and I_{max}/I_{min} (solid lines).

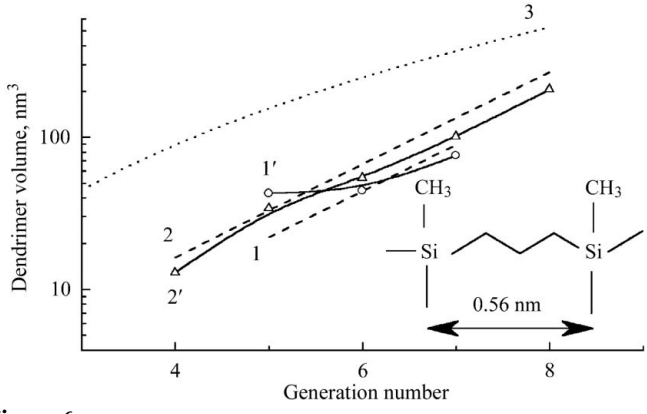

Figure 6
Dendrimer volume for $G^{(3)}$ (1, 1′) and $G^{(4)}$ (2, 2′) dendrimers of different generations found from bulk density measurements (1, 2) and *DAMMIN* (1′, 2′). The upper curve (3) presents the limiting volume of a ball with a radius equal to a fully straightened dendrimer's branch calculated from the known chemical structure (inset).

In the models generated, the interior of the dendrimers is potentially available for solvent molecule penetration (inclusion). Indeed, the overall envelope volumes of the equivalent ellipsoid (*SASHA*) exceeded the partial volumes of the bead-model body (*DAMMIN*) for all the dendrimers studied in this work (see Figs. 3 and 4, and Table 1). This leads to the conclusion that a fraction of about 0.2 of the overall volume for the $G^{(3)}$-type dendrimers and of about 0.3 for the $G^{(4)}$-type dendrimers is not filled with the beads, forming holes inside the dendrimer structure. This fraction of the overall volume is thus available for solvent penetration. Earlier, the value of 0.3–0.4 was estimated for the same parameter from the absolute intensity measurements of SANS and from the precise solution density measurements for $G^{(3)}$-type dendrimers studied in this work (Kuklin *et al.*, 2002, 2003). Somewhat higher values of the same parameter (0.43−0.58) were calculated in the study of the effect of solvent quality on the molecular dimensions of PAMAM dendrimers (Topp *et al.*, 1999), for the rather enlarged eighth generation of the PAMAM-type dendrimers.

The cross-section views of the models restored by *DAMMIN* revealed a pronounced heterogeneity within the dendrimer structure (Figs. 3 and 4). The density deficit was observed in the central part and also close to the periphery of the $G^{(3)}$-type and the $G^{(4)}$-type structures. We therefore believe that the usual assumption of radial symmetry of the density distribution inside the dendrimer structure is a rather coarse approximation. Neglecting the angular dependence of the density distribution may lead to oversimplification of the results.

Nevertheless, it is interesting to see to what extent the heterogeneous shape of the dendrimers restored in this work correlates with the averaged characteristics reported for the dendrimer architecture earlier (while neglecting the angular dependence of the density distribution inside dendrimer).

The results in Fig. 8 present the averaged radial distribution functions $\rho(R)$ for the studied dendrimers calculated by direct counting of the beads inside the volume of an appropriate spherical layer for the model bodies in Figs. 3 and 4. One can recognize that the averaged radial density distribution functions in Fig. 8 are consistent with the results of the comprehensive investigation published elsewhere for the PAMAM-type dendrimers (Prosa *et al.*, 2001). The revealed non-uniform radial density distribution (see curves 5–8 in Fig. 8), referred to as '... erratic behaviour' in the above-cited paper, appears to be a general feature of the dendrimers of different

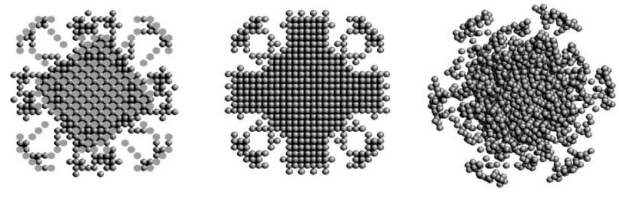

Figure 7
Shape determination for the $G^{(4)}7$ dendrimer. From left to right: equatorial cross section, front view and diagonal view. Prepared using *DAMMIN*. Predefined symmetry *P*432.

chemical structure. Besides, the density profile for the $G^{(4)}4$ dendrimer (curve 4 in Fig. 8) has a Gaussian form similar to that reported in another comprehensive study (Likos *et al.*, 2002). In our case, the Gaussian-like density distribution profile is the simple consequence of the density distribution averaging for the anisotropic spatial structure [$G^{(4)}4$ in Fig. 4].

To extend our comparison, the correlation function of the particle $\gamma(R)$ was determined by calculation of the averaged self-convolutions of the $\rho(R)$ functions from Fig. 8,

$$\gamma(R) = \langle \rho(R)\rho(-R) \rangle,$$

as well as the pair distance distribution functions of the scattering particles,

$$p(R) = R^2\gamma(R).$$

The pair distance distribution functions, $p(R)$, of some of the dendrimers are presented in Fig. 9.

It seems that the shape of the $p(R)$ functions in Fig. 9 is consistent with the well known shape in the literature (Rebrov *et al.*, 1998; Prosa *et al.*, 2001) for the other types of dendrimers. The bell-shaped $p(R)$ functions in Fig. 9 are typical for uniform globular or ball-like scattering particles (Feigin & Svergun, 1987). At the same time, one should recognize that the $p(R)$ functions in Fig. 9 found for the heterogeneous model bodies in Figs. 3 and 4 do not reflect the peculiarities of their inner spatial structure. Thus, the conclusion of a ball-like view of a single dendrimer in solution may be oversimplified. A more complex dendrimer structure lacking the radial symmetry gives more insight into the real dynamics and potential practical applications of the dendrimer macromolecules.

It is evident that the simple model of radial growth of the dendrimer branches cannot explain the observed anisometric shape and heterogeneity of the dendrimers, both with three and with four branches. At the same time, the peculiarities of the dendrimer structure for the two cases can be easily explained if one assumes the possibility of a branch director divergence from the ideal radial direction. Such a divergence looks like a spiralization of the dendrimer branches and can be treated in common terms of a 'persistent' flexibility of macromolecules. The scheme of such an arrangement has been published elsewhere (Ozerin *et al.*, 2004).

Of course, the restored shape of the dendrimer corresponds to an averaged structure including possible fluctuations in shape, in particular for the low dendrimer generations (Harries *et al.*, 2003; Ballauff & Likos, 2004). It is currently difficult to involve the notion of fluctuations in SANS and SAXS data treatment, as these computations are based on molecular dynamics or Monte Carlo calculations and not on real experiments on the dynamical behaviour of dendrimers (such as spin-echo or dynamic light scattering measurements). Regarding the question 'to what extent could fluctuations or sample heterogeneity influence the results', one should note that the *ab initio* SAXS/SANS models are low-resolution models reflecting the (averaged) overall shape. Given the resolution, the modelling employed does not require ideal ordering (identity of the dendrimers at the atomic level) and the models are thus fully compatible with the fluctuating dendrimers. The *ab initio* dendrimer models presented here are not 'snapshots' of the individual dendrimer structure (and this is the limitation of the low-resolution SAXS/SANS method), but emerge from the average over the ensemble. As the present modelling does not employ *a priori* information, it provides an unbiased picture of the overall organization of the dendrimers, which, in particular, suggests a considerable non-sphericity of the dendrimer molecules.

The observed shape asymmetry of the fluctuating dendrimers could be readily rationalized by assuming that due to specific interactions with solvent molecules the stretching mode of a dendrimer's branch deformation is not equivalent to the reverse compressing mode (similar to the well known anharmonicity in vibrational transitions). The equilibrium point would then be shifted from a spherical symmetric model to a non-symmetric one. Recent publications accounting for explicit dendrimer–solvent interactions (Lin *et al.*, 2005) yield results on different dynamics of the buried solvent molecules well inside of the dendrimer surface, and those well outside of the dendrimer, giving the physical background to suppose non-equivalence of the stretching and compressing deformation modes.

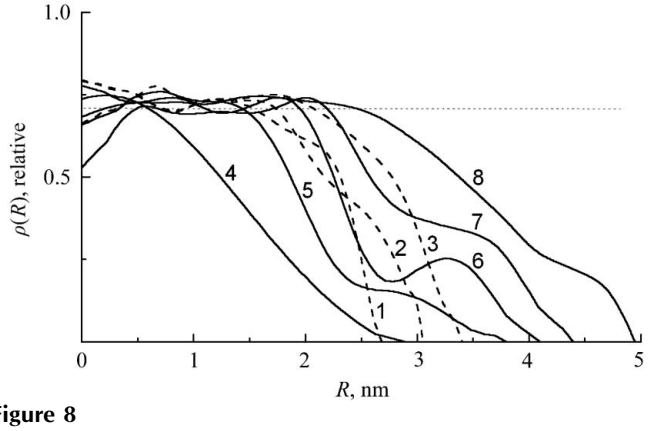

Figure 8
Radial density distribution functions $\rho(R)$ calculated for the bead-model bodies in Figs. 3 and 4: $G^{(3)}5$ (1), $G^{(3)}6$ (2), $G^{(3)}7$ (3), $G^{(4)}4$ (4), $G^{(4)}5$ (5), $G^{(4)}6$ (6), $G^{(4)}7$ (7) and $G^{(4)}8$ (8). The horizontal dotted line represents the relative hexagonal packing density of the beads inside model bodies.

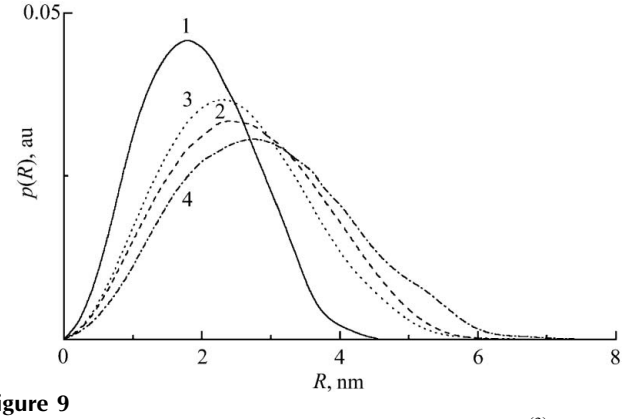

Figure 9
Distance distribution functions $p(R)$ of the dendrimers: $G^{(3)}5$ (1), $G^{(3)}7$ (2), $G^{(4)}5$ (3), $G^{(4)}7$ (4).

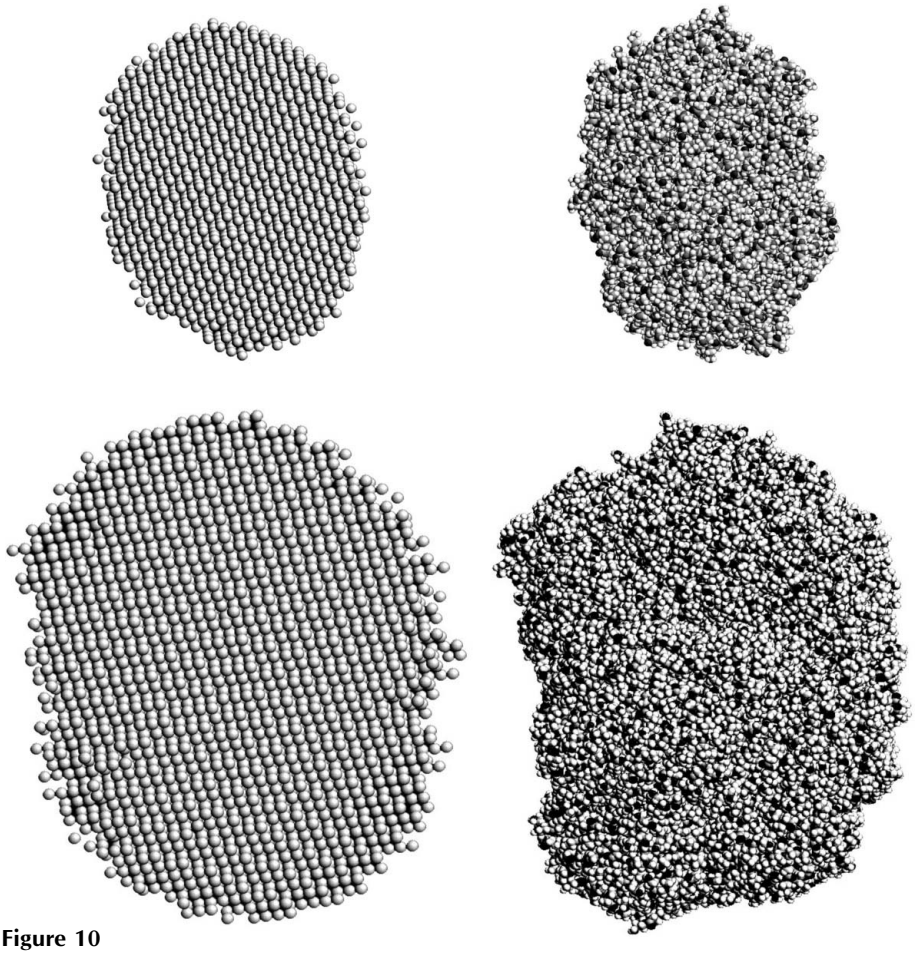

Figure 10
Shape determination for G8 (top) and G9 (bottom) PAMAM dendrimers. Left: *ab initio* shape provided by *DAMMIN*; right: instantaneous snapshots after long molecular dynamics simulations at T = 300 K (kindly provided by Dr P. K. Maiti). Space-filling rendering is used in both cases.

In recent publications of Maiti *et al.* (2004, 2005), comprehensive molecular dynamics simulations were performed on the structure of PAMAM dendrimers for generations 1 to 11. The computed models display an overall shape and anisometry similar to ours. To make a more quantitative comparison, we have digitized the earlier published SAS data from G8 and G9 PAMAM dendrimers (Prosa *et al.*, 1997; Nisato *et al.*, 2000) and reconstructed the shapes *ab initio* by the same procedure as described above for the polycarbosilane dendrimers. The shapes of the PAMAM dendrimers restored by *DAMMIN* are compared with the instantaneous snapshots after long molecular dynamics simulations in Fig. 10. The snapshots, calculated as described by Maiti *et al.* (2004), were kindly provided by Dr P. K. Maiti.

The astonishingly good agreement between the independent theoretical and experimental models constitutes a strong argument in favour of the results presented here and further underlines the potential of *ab initio* modelling as applied to the study of dendrimers.

4. Conclusion

In the present study, low-resolution shapes of polycarbosilane dendrimers with the three-functional and the four-functional branching centre reconstructed *ab initio* from small-angle scattering data reveal anisometric structures permeable to the solvent.

The angular dependence of the mass distribution function inside the dendrimers appears therefore to be important in accounting for the earlier reported controversy between the dendrimer structure and dynamics observed by various experimental methods and numerical calculations. Until now, the experimental results were mostly interpreted assuming the dendrimer structure to be radially symmetric leading to either the so-called 'dense-shell' model or to the 'dense-core' or uniform model. These models, as suggested by our results, may be an oversimplification of the real situation.

The above measurements of the solvent amount located in a 'confined geometry' inside the dendrimer structure allow one to devise new experiments on practical applications of the dendrimers based on the principles of host–guest and supramolecular chemistry.

The authors are thankful to Professor Aziz Muzafarov for making available a range of dendrimer materials. We thank Dr Prabal K. Maiti for the snapshots of the G8 and G9 PAMAM dendrimers presentation and for useful discussions. This work was funded by the Russian Foundation for Basic Research (grant No. 02-03-32867) and by the Russian Academy of Science (Chemistry and Materials Science Department, Objective Program No. 4).

References

Ballauff, M. & Likos, C. N. (2004). *Angew. Chem. Int. Ed. Engl.* **43**, 2998–3020.
Feigin, L. A. & Svergun, D. I. (1987). *Structure Analysis by Small-Angle X-ray Scattering and Neutron Scattering.* New York: Plenum Press.
Fréchet, J. M. J. & Tomalia, D. A. (2001). Editors. *Dendrimers and Other Dendritic Polymers.* Chichester: John Wiley.
Harries, H. M., Likos, C. N. & Ballauff, M. (2003). *J. Chem. Phys.* **118**, 1979–1988.
Konarev, P. V., Petoukhov, M. V. & Svergun, D. I. (2001). *J. Appl. Cryst.* **34**, 527–532.
Konarev, P. V., Volkov, V. V., Sokolova, A. V., Koch, M. H. J. & Svergun, D. I. (2003). *J. Appl. Cryst.* **36**, 1277–1282.
Kozin, M. B. & Svergun, D. I. (2001). *J. Appl. Cryst.* **34**, 33–41.
Kuklin, A. I., Ignat'eva, G. M., Ozerina, L. A., Islamov, A. Kh., Mukhamedzyanov, R. I., Shumilkina, N. A., Myakushev, V. D.,

Sharipov, E. Yu., Gordeliy, V. I., Muzafarov, A. M. & Ozerin, A. N. (2002). *Polym. Sci. A*, **44**, 2124–2133.
Kuklin, A. I., Ozerin, A. N., Islamov, A. Kh., Muzafarov, A. M., Gordeliy, V. I., Rebrov, E. A., Ignat'eva, G. M., Tatarinova, E. A., Mukhamedzyanov, R. I., Ozerina, L. A. & Sharipov, E. Yu. (2003). *J. Appl. Cryst.* **36**, 679–683.
Likos, C. N., Rosenfeldt, S., Dingenouts, N., Ballauff, M., Lindner, P., Werner, N. & Vögtle, F. (2002). *J. Chem. Phys.* **117**, 1869–1877.
Likos, C. N., Schmidt, M., Löwen, H., Ballauff, M., Pötschke, D. & Lindner, P. (2001). *Macromolecules*, **34**, 2914–2920.
Lin, S. T., Maiti, P. K. & Goddard, W. A. III (2005). *J. Phys. Chem. B*, **109**, 8663–8672.
Maiti, P. K., Çağın, T., Wang, G. & Goddard, W. A. III (2004). *Macromolecules*, **37**, 6236–6254.
Maiti, P. K., Çağın, T., Lin, S. T. & Goddard, W. A. III (2005). *Macromolecules*, **38**, 979–991.
Mallamace, F., Canetta, E., Lombardo, D., Mazzaglia, A., Romeo, A., Monsù Scolaro, L. & Maino, G. (2002). *Physica A*, **304**, 235–243.
Nisato, G., Ivkov, R. & Amis, E. J. (2000). *Macromolecules*, **33**, 4172–4176.
Ozerin, A. N., Muzafarov, A. M., Gordeliy, V. I., Kuklin, A. I., Ignat'eva, G. M., Krykin, M. A., Ozerina, L. A., Shumilkina, N. A., Islamov, A. Kh., Sharipov, E. Yu. & Mukhamedzyanov, R. I. (2003). *Macromol. Symp.* **195**, 171–178.
Ozerin, A. N., Muzafarov, A. M., Kuklin, A. I., Islamov, A. Kh., Gordelyi, V. I., Ignat'eva, G. M., Myakushev, V. D., Ozerina, L. A. & Tatarinova, E. A. (2004). *Dokl. Chem.* **395**, 59–62.
Ponomarenko, S. A., Rebrov, E. A., Boiko, N. I., Muzafarov, A. M. & Shibaev, V. P. (1998). *Polym. Sci. A*, **40**, 763–774.
Prosa, T. J., Bauer, B. J., Amis, E. J., Tomalia, D. A. & Scherrenberg, R. (1997). *J. Polym. Sci. Part B Polym. Phys.* **35**, 2913–2924.
Prosa, T. J., Bauer, B. J. & Amis, E. J. (2001). *Macromolecules*, **34**, 4897–4906.
Ramzi, A., Scherrenberg, R., Joosten, J., Lemstra, P. & Mortensen, K. (2002). *Macromolecules*, **35**, 827–833.
Rebrov, A. V., Fadeev, M. A. & Ozerin, A. N. (1998). *Dokl. Chem.* **360**, 88–91.
Sagidullin, A. I., Muzafarov, A. M., Krykin, M. A., Ozerin, A. N., Skirda, V. D. & Ignat'eva, G. M. (2002). *Macromolecules*, **35**, 9472–9479.
Scherrenberg, R., Coussens, B., van Vliet, P., Edouard, G., Brackman, J., de Brabander, E. & Mortensen, K. (1998). *Macromolecules*, **31**, 456–461.
Svergun, D. I. (1991). *J. Appl. Cryst.* **24**, 485–492.
Svergun, D. I. (1992). *J. Appl. Cryst.* **25**, 495–503.
Svergun, D. I. (1999). *Biophys. J.* **76**, 2879–2886.
Svergun, D. I., Volkov, V. V., Kozin, M. B. & Stuhrmann, H. B. (1996). *Acta Cryst.* A**52**, 419–426.
Tatarinova, E. A., Rebrov, E. A., Myakushev, V. D., Meshkov, I. B., Demchenko, N. V., Bystrova, A. V., Lebedeva, O. V. & Muzafarov, A. M. (2004). *Russ. Chem. Bull. Int. Ed.* **53**, 2591–2600.
Topp, A., Bauer, B. J., Tomalia, D. A. & Amis, E. J. (1999). *Macromolecules*, **32**, 7232–7237.
Volkov, V. V. & Svergun, D. I. (2003). *J. Appl. Cryst.* **36**, 860–864.